NJC

Accepted Manuscript

This article can be cited before page numbers have been issued, to do this please use: D. Barrera, F. G. D. Mendonça, A. H. Castro, J. P. de Mesquita, R. M. Lago and K. Sapag , *New J. Chem.*, 2018, DOI: 10.1039/C8NJ00922H.

ROYAL SOCIETY OF CHEMISTRY

rsc.li/njc

View Article Online
DOI: 10.1039/C8NJ00922H

New Journal of Chemistry

ARTICLE

Surface modified mesoporous nanocast carbon as catalyst for aqueous sulfide oxidation and adsorption of produced polysulfides

Received 00th January 20xx,
Accepted 00th January 20xx

DOI: 10.1039/x0xx00000x

www.rsc.org/

Deicy Barrera,[a] Fernanda Gomes de Mendonça,[b] Arthur Henrique de Castro,[c] João Paulo de Mesquita,[c] Rochel Montero Lago,*[b] and Karim Sapag *[a]

In this work, a mesoporous nanocast carbon prepared using SBA-15 as template was modified by surface oxidation to produce unique catalysts for sulfide oxidation/elimination from the aqueous medium. Different characterization techniques (BET, SEM, Raman, FTIR, potentiometric titration, elemental analyses, cyclic voltammetry) showed that treatment with concentrated HNO_3 at 80 °C for 5, 15 and 30 min attacks the carbon structure creating different oxygen surface functionalities in concentrations varying from 0.4-1.1 mmol g^{-1} with small effect on surface area (1080-1148 m^2g^{-1}) and pore volumes (micropore 0.17-0.20 cm^3g^{-1} and mesopores 0.36-0.50 cm^3g^{-1}). These materials showed high activities for the oxidation of sulfide in aqueous medium forming polysulfides, e.g., S_2^{2-}, S_3^{2-} and S_4^{2-}, which are rapidly eliminated from the aqueous medium. These results are discussed regarding efficient sulfide oxidation at redox surface oxygen sites leading to the formation of higher polysulfides followed by adsorption of these relatively large and more hydrophobic molecules into the mesopores.

1. Introduction

Nanocasting is a versatile technique to create nanostructured carbons (NC) with controlled morphologies, high surface areas, narrow pore size distributions and high pore volumes.[1-5] Different templates, such as zeolites,[6] pillared clays,[7] and silica,[8] have been used to produce NC with different pore sizes and geometries with a high structural ordering. The use of mesoporous silicas, e.g., SBA-15, as a template for the production of a mesoporous carbon named CMK-3 has been reported in several works.[8-10] These hierarchical carbon nanorods CMK-3 with a hexagonal network have been used in different applications such as adsorption,[11] catalysis,[12] gas separation process,[13] gas storage,[14] gas capture,[15] and electrodes in lithium batteries.[16]

In this work, the mesoporous surface of a hierarchical carbon was modified by oxidation with HNO_3 to produce unique catalytic materials for the oxidation of sulfides in an aqueous medium.

Sulfide in aqueous medium, mainly as H_2S, is a serious problem due to odor, hazardous issues, and corrosion of equipment and infrastructure.[17-20] In this context, the elimination of sulfide from wastewaters is of considerable importance.[21]

The removal of hydrogen sulfide from the gas phase has been extensively investigated by different processes, mainly by air oxidation in the presence of different catalysts such as vanadium and iron oxides.[22,23] Silicon carbide foams containing carbon nanotubes also showed to be effective on the oxidation of H_2S in the gas phase to elemental sulfur.[24] On the other hand, in aqueous media only a few studies have been carried out. Some microorganisms showed activity to oxidize different sulfur species in industrial wastewaters.[25-28] The oxidation activity of these bacteria has been related to the presence of quinone redox groups and a facile electron transportation system in the enzyme sulfide-quinone reductase.[29,30]

Inorganic synthetic catalysts based on ferrites MFe_2O_4 (M=Fe, Cu, Co) and composites carbon/Fe_3O_4 were investigated as catalysts for oxidation of aqueous sulfide.[31,32] Recent works showed that carbon-based materials, such as activated carbon, graphite and graphene have also shown high activity for the oxidation of aqueous sulfide.[33-35] These results suggested that important features to produce active catalysts are the presence of surface redox oxygen groups, e.g., quinone, combined with the graphene electron conducting structure. In these studies, the main reaction observed was the oxidation of sulfide to disulfide (S_2^{2-}).

Hereon, it is discussed some unique features of modified nanocast mesoporous carbon for the oxidation of aqueous sulfide, i.e., well defined mesoporous structure, the high

[a] Laboratorio de Sólidos Porosos, Instituto de Física Aplicada, CONICET, Universidad Nacional de San Luis, San Luis, Argentina. E-mail: sapag@unsl.edu.ar
[b] Departamento de Química, Universidade Federal de Minas Gerais, Belo Horizonte, Brazil. E-mail: rochel@ufmg.br
[c] Departamento de Química, Universidade Federal dos Vales do Jequitinhonha e Mucuri, Diamantina, Brazil.
Electronic Supplementary Information (ESI) available: [details of any supplementary information available should be included here]. See DOI: 10.1039/x0xx00000x

View Article Online
DOI: 10.1039/C8NJ00922H

oxidation activity compared to other carbon-based catalysts, the production of high polysulfides, e.g., S_3^{2-} and S_4^{2-} (Equation 1), and also the removal of these relatively large polysulfides from aqueous medium by adsorption in the mesopore space.

$$2S^{2-}_{aq} \rightarrow S_2^{2-}{}_{aq} \rightarrow S_3^{2-}{}_{aq} \rightarrow S_4^{2-}{}_{aq} \quad \text{(Equation 1)}$$

2. Experimental

2.1. Nanostructured Carbons (NC)

NC synthesis was carried out by a nanocasting process using different synthesis conditions reported elsewhere.[2,10] The NC obtained is a negative replica of the inorganic matrix. The synthesis of NC involves five main steps: (i) inorganic template synthesis, where the ordered mesoporous silica-based material SBA-15 was chosen; (ii) templated impregnation with sucrose as carbon source; (iii) polymerization; (iv) carbonization of the organic material and (v) template removal, where an acid treatment was used in this case. SBA-15 pores were filled with an aqueous solution of sucrose dissolved in sulfuric acid, used as a catalyst in the carbonization step, and water, in a mass ratio of 1:1.3:0.14:5 (SBA-15: sucrose: H_2SO_4: water). This mixture was stirred at room temperature for an hour, followed by a polymerization step drying at 100 °C for 6 h and subsequently, the temperature was raised to 160 °C for 6h. An additional impregnation was carried out to ensure the complete filling of SBA-15 porous structure. The carbonization step was performed by heating the composite from room temperature up to 900 °C in a N_2 atmosphere, with a heating rate of 3 °C/min. The resulting silica/carbon composite was in contact with a hydrofluoric solution (5 wt. %) at room temperature during 24 h to remove the SBA-15. Then the NC was filtered and washed up to a conductivity value smaller than 10 μS/cm and finally was dried at 80 °C for 12 h.[36]

2.2. Functionalized Nanostructured Carbons (FNC)

NC was treated with HNO_3 to introduce oxygen-containing functional groups. 15 mL of concentrated HNO_3 were added to 500 mg of NC heating in an oil bath at 80 °C during 5 minutes (FNC_5), 15 minutes (FNC_15) and 30 minutes (FNC_30). Afterward, samples were washed with abundant distilled water up to neutral pH to remove excess of acid and water-soluble products of oxidation. After washing, the materials were dried at 80 °C overnight.

2.3. Characterization and methods

NC and FNC materials were analyzed by X-ray diffraction (XRD) in a Bruker-AXS 2D Phaser equipment, with Cu-Kα radiation (λ = 1.54 Å). Morphological characterization of NC and FNC samples was carried out using scanning electronic microscopy (SEM) obtained in a LEO 1450 VP equipment with an energy dispersive X-ray probe (EDX) EDAX Genesis 2000. N_2 adsorption-desorption isotherms at 77 K were obtained in a manometric adsorption equipment (Micromeritics ASAP-2000). The specific surface area (S_{BET}) of all these materials was estimated by the Brunauer, Emmett and Teller method (BET) using N_2 adsorption data at 77 K for relative pressures between 0.05 and 0.2. The micropores ($V_{\mu P}$) and primary mesopores (V_{PMP}) volumes were evaluated by the αS-plot method. The total pore volume (V_{TP}) was obtained by Gurvich rule[37,38] at a relative pressure of 0.98. The pore size distributions of the studied materials were obtained by the QSDFT method included in AsiQwin software, v. 2.0 (Quantachrome Instruments) where the Kernel used was *''N_2 at 77 K on carbon (slit/cylindrical. Pore, QSDFT adsorption branch)''*. Transmission electron microscopy (TEM) image was obtained using a Philips CM200UT microscope. Raman spectra were obtained in a Senterra Bruker equipment, with an excitation wavelength of 633 nm, a laser spot size of 20 μm with confocal imaging microscope and power of 2 mW. Infrared spectra (IR) were recorded in a Bruker ALPHA equipment, in the wavelengths between 4000-400 cm^{-1}, with 64 scans per sample. Elemental analyses were performed in a Perkin Elmer 2400 equipment. Potentiometric titration curves were obtained in a SHOTT automatic titrator (Titroline 7000) with a combined pH electrode model N6280 (SHOTT), under nitrogen atmosphere to avoid contamination by dissolved atmospheric CO_2. For titrations, 10 mg of sample was dispersed in 20 mL of a solution 0.000083 mol L^{-1} HCl and titrated with a CO_2-free solution of NaOH (0.0116 mol L^{-1}). In order to keep H^+ ions activity constant during the experiments, ionic strengths of HCl and NaOH solutions were fitted to 0.10 mol L^{-1} by dissolution of sodium chloride. To determine the nature and amount of the acidic functional groups present on the surface of the samples a non-linear regression program was used.[39,40] Based on Lemos *et al.*,[33] kinetic studies were carried out monitoring the reaction at the wavelengths 273, 290 and 360 nm for the species S_2^{2-}, S_3^{2-} and S_4^{2-}, respectively. The reactions were performed with 10 mg of materials suspended in 6 mL of a solution of $Na_2S.9H_2O$ (8 g L^{-1}). Measures of electronic absorption UV-Vis were obtained using a Shimadzu UV 2550 spectrometer. Inductively coupled plasma optical emission spectroscopy (ICP-OES, Radial) was performed for the materials after sulfide oxidation in a spectrometer Arcos Spectro. Electrochemical measurements were obtained with bipotentiostat (DropSens) at room temperature using a conventional three electrode arrangement with a Pt wire counter electrode, an Ag/AgCl reference electrode (3.0 M KCl), and a carbon paste electrode as working electrode. First, 45 mg of graphite powder (Aldrich) was mixed with 5 mg of mineral oil nujol for 10 minutes. Then, 47.5 mg in this graphite paste was mixed with 2.5 mg of sample, and the resulting paste was packed into a 3 mm internal diameter (0.07cm^2). The electrical contact was made with a copper wire. The surfaces of electrodes were polished on paper to produce a flat reproducible working surface. All electrochemical experiments in this work were performed in a 0.1 M KCl solution as a supporting electrolyte.

3. Results and discussion

View Article Online
DOI: 10.1039/C8NJ00922H

The nanostructured carbon (NC) was obtained using SBA-15 mesoporous silica as template and sucrose as carbon source pyrolyzed at 900 °C, followed by silica removal by HF treatment. The obtained NC was treated with concentrated HNO_3 at *ca.* 80 °C for 5, 15 and 30 min and extensively washed with water.

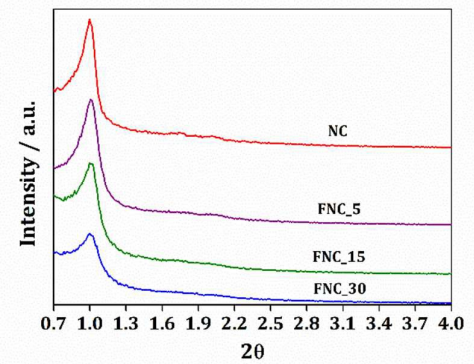

Fig. 1 Low-angle XRD patterns and of NC and FNC samples.

These samples are named hereon FNC_5, FNC_15, and FNC_30, respectively.

Low-angle XRD patterns (Fig. 1) showed for NC and FNC samples a well-resolved peak assigned to (100) diffractions of the 2D hexagonal space group, p6mm, (2θ ~ 1 °), indicating the preservation of the structure in the mesoporous carbon derived from SBA-15. SEM images obtained for NC and FNC samples presented similar rod-like morphologies suggesting that the HNO_3 treatment did not cause a significant change in the carbon texture (Fig. 2). The ordered mesoporous structure was also studied using TEM. In Fig. 2 can be seen a TEM micrograph image for NC viewed perpendicular to the direction of the hexagonal pore arrangement. The TEM image shows that the structure of NC is an inverse replica of SBA-15 (template), which consists of a hexagonal arrangement of cylindrical mesoporous tubes around of 8 nm in diameter with interconnection of tubes

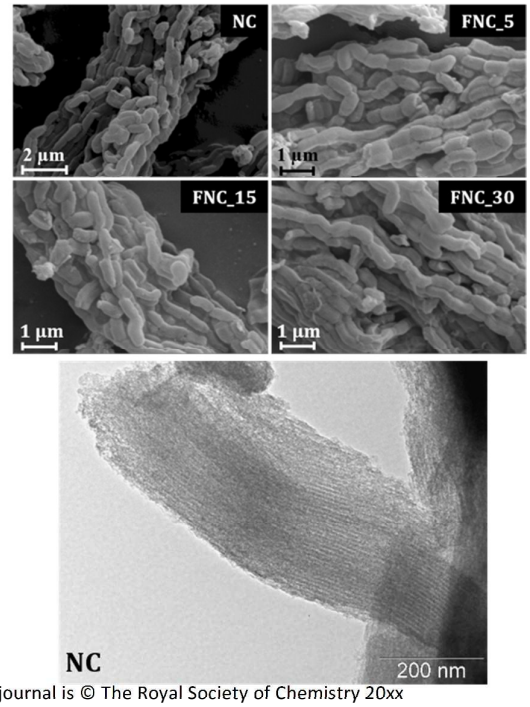

Fig. 2 SEM and TEM images obtained of NC and FNC samples.

Table 1. Textural properties of NC and FNC materials

Samples	S_{BET} [m^2/g]	$V_{\mu P}$ [cm^3/g]	V_{PMP} [cm^3/g]	V_{TP} [cm^3/g]
NC	1148	0.20	0.50	1.32
FNC_5	1080	0.17	0.33	1.16
FNC_15	1100	0.18	0.27	1.17
FNC_30	1080	0.18	0.36	1.05

by micropores present in the pore walls. For FNC samples, it can be assumed that their structures have not been drastically altered, due to the shape of the isotherms similar to the unmodified sample.

Nitrogen adsorption-desorption analyses (Supplementary Material) showed Type IV isotherms and an H2 type hysteresis loop, typical of mesoporous materials with a significant amount of micropores.[38] Textural properties of NC and FNC obtained from N_2 adsorption data at 77 K are shown in Table 1. It can be
observed that the original NC showed a specific surface area of 1148 m^2 g^{-1} with a relatively large primary mesoporous volume. As the NC was treated with HNO_3, the surface area slightly decreased to *ca.* 1080 - 1100 m^2 g^{-1} with a concomitant decrease of the micro and mesoporous volume. Pore size distributions (Supplementary Material) showed very similar results for the different samples, with approximately 50 % of total pores between 3.5 and 6 nm centered at 4.6 nm. Although the effect of the different pore sizes is not the core of this work, it is important to point out that the influence of larger or smaller mesopores sizes could affect the process.

Raman spectra of the obtained materials showed the two typical carbon bands: D band at *ca.* 1330 cm^{-1} (related to the presence of defects in the carbon structure) and G band centered in 1590 cm^{-1} (related to more organized less defective graphene structures).[41] As it can be seen in Fig. 3, I_D/I_G ratio for NC sample (0.86) is lower compared to FNC_15 and FNC_30 (1.05 - 1.32), indicating the formation of defects related to oxidation sites after reaction with HNO_3. The dimensions of non-defective graphene structures present in the carbon were

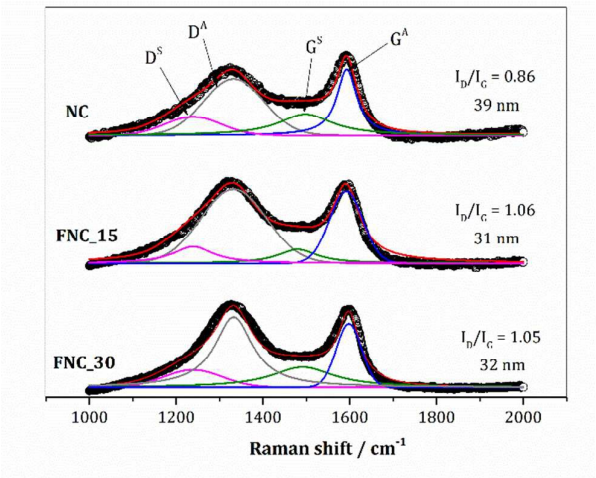

View Article Online
DOI: 10.1039/C8NJ00922H

Fig. 3 Raman spectra of NC and FNC samples with calculated I_D/I_G ratios and estimated dimensions of nondefective graphene structures.

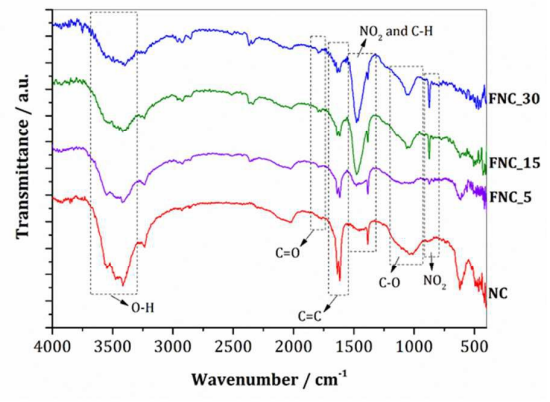

Fig. 4 IR spectra obtained for NC and FNC samples.

obtained from Raman spectra fitted according to the protocol described by Ribeiro-Soares *et al.*[42] Different component peaks were used: two Lorentzians (D^A and G^A peaks) and other two Gaussians (D^S and G^S peaks). D^S and G^S peaks introduced in this fitting come from highly disordered areas and are important to be considered specially when the sample presents small crystallite sizes (Fig. 3).[42] The obtained results indicated that the average dimension of the non-defective graphene structures decreased from 39 nm to 31-32 nm after oxidation, likely due to the attack/oxidation of the carbon structure.

Infrared spectra (IR) for NC sample (Fig. 4) showed bands between 3550 - 3400 cm^{-1} related to O-H groups, 1636 and 1617 cm^{-1} related to C=C bonds, and at *ca.* 1385 and 1050 cm^{-1} likely due to C-H and C-O from different functional groups, respectively. Upon oxidation, the presence of new bands at 1470 and 880 cm^{-1} indicates chemical functionalization with nitro groups (NO_2). It can also be noticed a decrease in the bands related to C=C bonds (1636 and 1617 cm^{-1}) and a C-H shoulder present near 1380 cm^{-1} due to the attack of nitric acid. The band near 1730 cm^{-1} suggests to the formation of carboxylic acids.[43]

Elemental analyses (CHN) showed for NC sample a carbon content of 89 %. After oxidation with HNO_3, the carbon content decreased to *ca*. 68 % and nitrogen content to *ca*. 0.9-1 % indicating an important oxidation of the carbon.

Potentiometric titrations were performed to estimate the nature and number of acid functional groups. Fig. 5 shows the concentration of groups for each material, according to their pKa. Obtained experimental data for the different samples are shown in Supplementary Material.

The obtained results suggest the presence of three representative functional groups: carboxylic acid, lactone, and phenol.[44] As expected, NC presented less acid functional groups than functionalized materials. As the NC was treated with HNO_3 for 5, 15 and 30 min, it was observed a gradual increase in the concentration of the different functional groups. It is interesting to observe that especially the groups with pKa higher than 8 (related to phenols and quinones) and in the range 4-6 (related to carboxylic groups) showed a more significant increase.

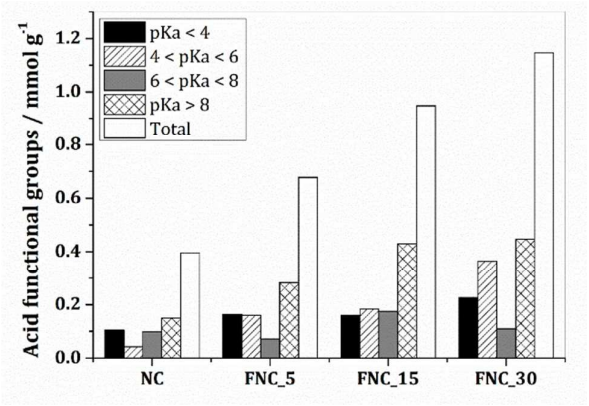

Fig. 5 Number of functional groups according to pKa, and total acid functional groups in NC and FNC samples.

3.1. Kinetic studies of sulfide oxidation

Previous works showed that the oxidation of aqueous Na_2S in the presence of different carbons resulted in several changes in the UV-Vis spectrum.[33-35] Fig. 6 shows the UV-Vis spectra obtained for sulfide oxidation in the presence of the carbon FNC_15 at different times. Na_2S solution in the presence of the carbon materials produced UV-Vis absorption bands at the wavelengths 273, 290 and 375 nm, suggesting the oxidation of sulfides to different polysulfides, e.g., S_2^{2-}, S_3^{2-} and S_4^{2-}, respectively.[33,34] A progressive increase in absorbance was observed up to 10 minutes of reaction. After 15 up to 20 minutes, the absorbance of all bands strongly decreased.

These results can be better visualized by the absorption band at 273 nm (Fig. 7). It can be seen that the absorbance of all materials increased at the beginning of reaction indicating the oxidation to form S_2^{2-} species. However, after 5-15 min the absorbance at 273 nm strongly decreased.

The absorbances for different polysulfide species S_2^{2-}, S_3^{2-} and S_4^{2-} estimated by deconvolution of spectra for FNC_15 after 5, 10, 15 and 20 minutes of reaction are shown in Supplementary Material. The relative spectral areas for the different species produced during reaction with FNC_15 are

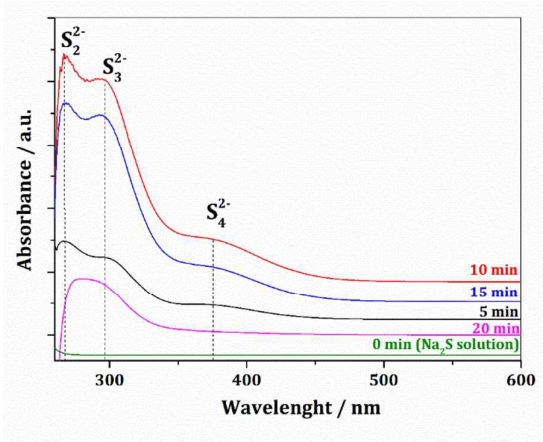

View Article Online
DOI: 10.1039/C8NJ00922H
Journal Name ARTICLE

Fig. 6 Monitoring of sulfide oxidation by UV-Vis spectroscopy for FNC_15 with Na_2S

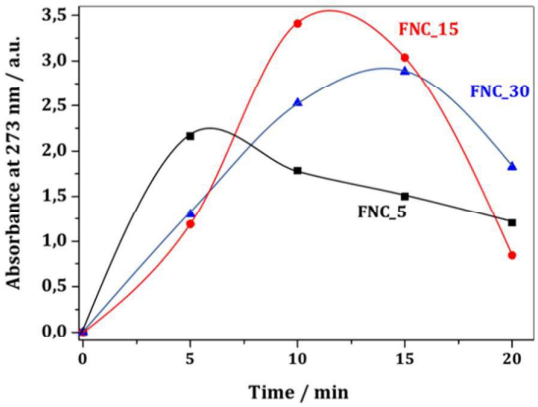

Fig. 7 Kinetics of sulfide oxidation for FNC_5, FNC_15, and FNC_30 monitored by the absorbance at 273 nm.

The absorbances for different polysulfide species S_2^{2-}, S_3^{2-} and S_4^{2-} estimated by deconvolution of spectra for FNC_15 after 5, 10, 15 and 20 minutes of reaction are shown in Supplementary Material. The relative spectral areas for the different species produced during reaction with FNC_15 are shown in Fig. 8. It can be observed that absorbance for all species increased simultaneously up to 10 - 15 min, but also decreased simultaneously reaching very low values near 20 min. Although the reason for this decrease is not clear, it can be related to a sequential process of polysulfide formation followed by adsorption on the porous carbon surface (Equation 2). In fact, sulfur analyses by ICP-OES after the reactions showed 2.54, 4.61, and 3.71% of S for FNC_5, FNC_15 and FNC_30, respectively.

S^{2-}_{aq} → Polysulfide $S_n^{2-}{}_{aq}$ → adsorption on carbon surface (Equation 2)

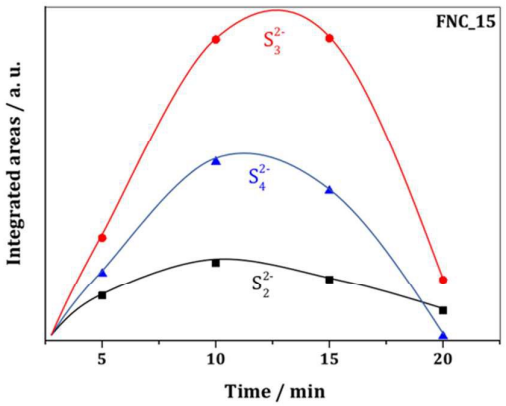

Fig.8 Relative spectral areas of bands related to the species S_2^{2-}, S_3^{2-} and S_4^{2-} during reaction time with material FNC_15.

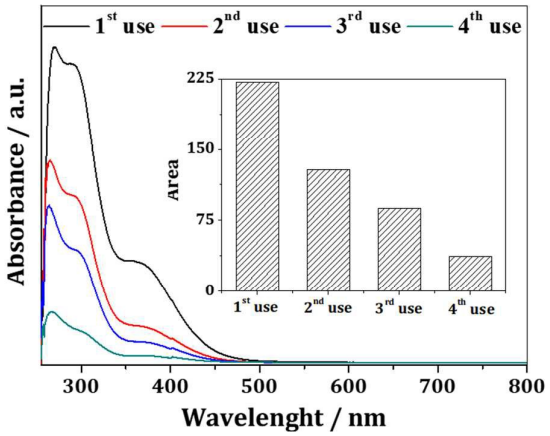

Fig. 9 UV-Vis spectra for sulfide oxidation in the presence of FNC_15 obtained at 10 min reaction in the 1st, 2nd, 3rd and 4th uses (Inset: integrated areas under the spectrum of each reuse).

It was investigated the reuse of the carbon in consecutive reactions in order study the deactivation of the catalysts. The obtained results are shown in Fig. 9. It can be observed by the UV-Vis spectra obtained at 10 min reaction that all the bands gradually decreased during the 1st, 2nd, 3rd, and 4th uses, indicating a deactivation.

The efficiency of NC and FNC materials for sulfide oxidation was compared to AC (commercial activated carbon),[33] graphene/graphite[34] and a high surface area carbon made of mesophase pitch.[35] Fig. 10 shows the comparison, which was performed based on the formation of S_2^{2-} by the absorption at 273 nm after 10 min reaction. It can be observed that as NC is oxidized with HNO_3 for 5 and 15 min the activity strongly increased. On the other hand, oxidation of NC for 30 min led to a decrease in sulfide conversion. Microporous commercial activated carbon made of coconut shell (before and after HNO_3 oxidation),[33] graphene and graphite[34] showed much lower activities for sulfide oxidation. Only an activated carbon with a surface area of 3250 m^2 g^{-1} showed sulfide oxidation activity comparable to FNC_15.[35]

In order to investigate the catalytic effect of the carbon surface on the oxidation of sulfide, cyclic voltammetry

Fig. 10 Formation of S_2^{2-} in the presence of different carbon materials measured under the same condition by the absorbance at 273 nm after 10 min of reaction.

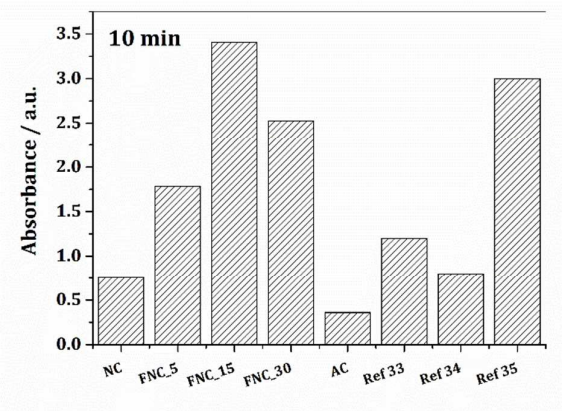

View Article Online
DOI: 10.1039/C8NJ00922H

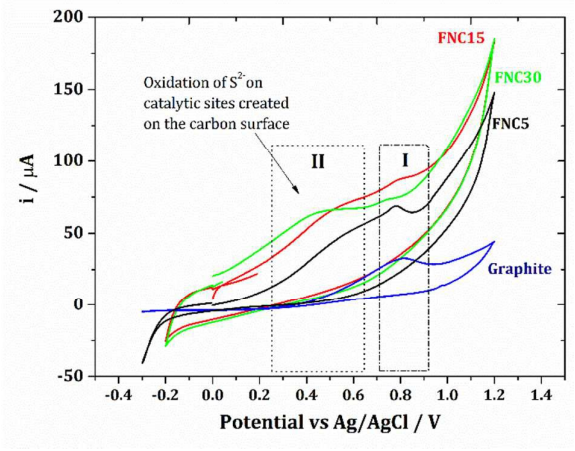

Fig. 11 Cyclic voltammograms obtained for FNC samples and graphite (Na_2S 0.001 M solutions, 25 mVs^{-1}).

experiments were carried out (Fig. 11). It was first investigated the effect of the oxidative treatments on the capacitive currents of the electrodes prepared with the different materials. The obtained results clearly showed an increase in the capacitive
currents with the oxidation of the carbon materials (Supplementary Material). The capacitance of the carbon materials is governed mainly by the textural properties (porosity, surface area) and surface chemistry.[45] The increased concentration of oxygenated functional groups modifies the electrostatic field of the surface, increasing the polarity, providing a greater interaction with the water molecules.[46] In addition, many oxygenated functional groups may undergo redox reactions and generate a capacitive pseudo-current.[47] Fig. 11 shows for the electrode prepared only with graphite a well-defined irreversible anodic peak around 0.80 V (Peak I) attributed to the oxidation of the aqueous sulfide. The linear relationship between the anodic peak currents and the square root of the scan rate suggests a diffusion controlled electrode reaction (Supplementary Material). The modification of the graphite paste electrode with samples of mesoporous nanocast carbon led to a widening of the oxidation peak hampering the definition of the peak, but indicating a lower sulfur initial oxidation potential for the samples treated with HNO_3. It is also possible to verify that the voltammograms of the modified electrodes present two oxidation regions, one near 0.80 V, promoted by the surface of the graphite, and another that is initiated at lower potentials generated by the surface of the oxidized mesoporous nanocast carbon. These results indicate a clear catalytic effect.

3.2. Preliminary discussion on the reaction mechanism

The FNC carbon catalysts present in this work show two unique features, i.e., the formation of large amounts of high polysulfides (S_3^{2-} and S_4^{2-}) and a consecutive adsorption of these polysulfides.

Previous works[31-35] suggested that the mechanism of aqueous S^{2-} oxidation probably involves the interaction with redox groups on the carbon surface, forming intermediate oxidized species. In this step, electronic transferences may occur from S^{2-} species to the graphene conducting structure. Sulfur oxidized species can then react with another S^{2-} producing disulfides or higher polysulfides. Besides these surface redox groups, the conducting carbon graphene structure was suggested to be important to transfer the electrons involved in the reaction.[31-35] Upon extensive HNO_3 oxidation, a large number of defects created in the graphene structure might affect electron conductivity. This probably explains the decrease in sulfur oxidation activity for the catalyst FNC_30 compared to FNC_15.

Another aspect of carbon catalysts to be considered is the pore structure, which likely controls the reaction by the diffusion limitations of sulfur species in and out of the pores.[35] The diffusion of aqueous S^{2-} species is likely more difficult in small pores, especially due to the presence of negative surface charge of oxygen functionalities, such as carboxylic $(-COO^-)_{surf}$ and phenolic$(-O^-)_{surf}$. In this context, larger mesopores should facilitate the access of S^{2-} species to the surface to form the primary reaction product S_2^{2-}. Moreover, with more S^{2-} and enough space inside the pores, S_2^{2-} can react with other S^{2-} species to form higher polysulfides, e.g., S_3^{2-} and S_4^{2-}. In fact, despite the relatively high specific surface area (890 $m^2\ g^{-1}$), and similar concentration and type of oxygen surface groups, commercial microporous AC showed the formation of only S_2^{2-} and very low sulfide oxidation activity compared to all FNC samples. This is likely related to the hindering of the reaction in the micropores (diameter < 2 nm) that is limited by the diffusion of the reactant and products with relatively large molecular sizes (S_2^{2-}, S_3^{2-} and S_4^{2-} molecular diameters of *ca.* 0.4, 0.6 and 0.8 nm, respectively).[40,48] Fig. 12 shows a schematic representation of this process inside micro and mesopores.

Conclusions

The results presented in this work showed that mesoporous nanocast carbon modified by controlled oxidation with HNO_3 are unique catalysts for the oxidation of sulfide in aqueous medium. Some of the unique features of the catalyst are: (i) higher activities compared to other carbon based catalysts reported in the literature, (ii) formation of large amounts of higher polysulfides S_3^{2-} and S_4^{2-} and (iii) removal of these

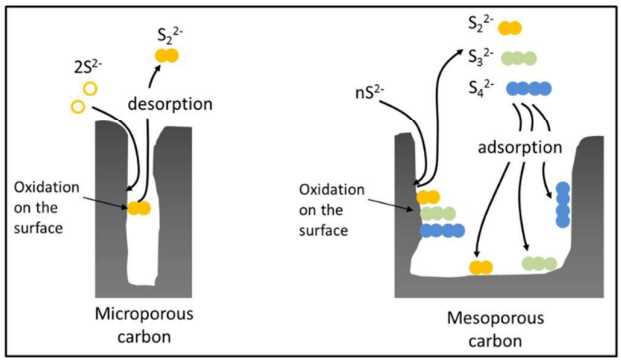

DOI: 10.1039/C8NJ00922H

Fig. 12 Schematic representation of the limited reaction of S^{2-}_{aq} in micropores compared to the production and adsorption of higher polysulfides in mesopores.

polysulfides by consecutive adsorption. These features are likely produced by the combination of a relatively high surface area modified with active redox oxygen groups. It is proposed that the presence of significant mesoporosity is very important to
afford enough space for the consecutive oxidation of S^{2-} to polysulfides and also for their posterior adsorption.

Conflicts of interest

There are no conflicts to declare.

Acknowledgments

Authors thank the financial support of INCT-MIDAS, Universidade Federal de Minas Gerais, Fundep, FAPEMIG, CNPq and CAPES. To LABPEMOL for low-angle XRD analysis. Deicy Barrera and Karim Sapag gratefully acknowledge Universidad Nacional de San Luis and CONICET.

Notes and references

1. A. H. Lu and F. Schüth, *Adv. Mater.*, 2006, **18,** 1793-1805.
2. Y. Xia, Z. Yang and R. Mokaya, *Nanoscale*, 2010, **2**, 639-659.
3. D. Tiwari, H. Bhunia and P. K. Bajpai, *Appl. Surf. Sci.*, 2017, **414**, 380-389.
4. X. Hu, L. Huang, J. Zhang, H. Li, K. Zha, L. Shi and D. Zhang, *J. Mater. Chem. A*, 2018, **6**, 2952-2963.
5. Y. Cao, M. Lu, J. Fang, L. Shi and D. Zhang, *Chem. Commun.*, 2017, **53**, 7549-7552.
6. Z. Ma, T. Kyotani and A. Tomita, *Carbon*, 2002, **40**, 2367-2374.
7. G. Sandí, P. Thiyagarajan, K. A. Carrado and R. E. Winans, *Chem. Mater.*, 1999, **11**, 235-240.
8. A. Galarneau, H. Cambon, F. Di Renzo, R. Ryoo, M. Choib and F. Fajula, *New J. Chem.*, 2003, **27**, 73-79.
9. P. A. Russo, M. M. L. R. Carrott and P. J. M. Carrott, *New J. Chem.*, 2011, **35**, 407-416.
10. M. Regiart, J. L. Magallanes, D. Barrera, J. Villarroel-Rocha, K. Sapag, J. Raba and F. Bertolino, *Sens. Actuators, B*, 2016, **232**, 765-772.
11. D. Saha and S. Deng, *J. Colloid Interface Sci.*, 2010, **345**, 402-409.
12. M. J. Kim, T. W. Kim, H. J. Chae, C. U. Kim, S. Y. Jeong, J. R. Kim and K. S. Ha, *J. Nanosci. Nanotechnol.*, 2016, **16**, 2004-2009.
13. X. Peng, D. Cao and W. Wang, *Chem. Eng. Sci.*, 2011, **66**, 2266-2276.
14. E. Kockrick, C. Schrage, L. Borchardt, N. Klein, M. Rose, I. Senkovska and S. Kaskel, *Carbon*, 2010, **48**, 1707-1717.
15. H. Seema, K. Kemp, N. Le, S. W. Park, V. Chandra, J. W. Lee, K. Kim, *Carbon*, 2014, **66**, 320-326.
16. P. G. Bruce, S. A. Freunberger, L. J. Hardwick and J. M. Tarascon, *Nat. Mater.*, 2012, **11**, 19 – 29.
17. J. E. Burgess, S. A. Parsons and R. M. Stuetz, *Biotech. Adv.*, 2011, **19**, 35-63.
18. G. Tchobanoglous, F. L. Burton and H. D. Stensel, *Wastewater Engineering: Treatment and Reuse*, fourth ed., Metcalf & Eddy, Inc., New York, 2003.
19. R. J. Llansó, *J. Exp. Mar. Biol. Ecol.*, 1991, **153**, 165-178.
20. M. S. Wiener, B. V. Salas, M. Quintero-Núñez and R. Zlatev, *Corros. Eng. Sci. Technol.*, 2006, **41**, 221-227.
21. L. Zhang, P. De Schryver, B. De Gusseme, W. De Muynck, N. Boon and W. Verstraete, *Water Res.*, 2008, **42**, 1-12.
22. M. León, J. Jiménez-Jiménez, A. Jiménez-López, E. Rodríguez-Castellón, D. Soriano and J. M. López Nieto, *Solid State Sci.*, 2010, **12**, 996-1001.
23. V. D. Kapse, S. A. Ghosh, F. C. Raghuwanshi and S. D. Kapse, *Mater. Chem. Phys.*, 2009, **113**, 638-644.
24. C. Duong-Viet, H. Ba, Z. El-Berrichi, J. M. Nhut, M. J. Ledoux, Y. Liu and C. Pham-Huu, *New J. Chem.*, 2016, **40**, 4285-4299.
25. M. R. Hoffmann and B. C. Lim, *Env. Sci. Technol.*, 1979, **13**, 1406-1414.
26. S. Zhang, R. Bao, J. Lu and W. Sang, *Sep. Purif. Technol.*, 2018, **195**, 314-321.
27. J. Macy, I. Schröder, R. Thauer and A. Kröger, Arch. *Microbiol.*, 1986, **144**, 147-150.
28. P. F. Henshaw and W. Zhu, *Water Res.*, 2001, **35**, 3605-3610.
29. C. G. Friedrich, D. Rother, F. Bardischewsky, A. Quentmeier and J. Fischer, *Appl. Environ. Microbiol.*, 2001, **67**, 2873-2882.
30. M. Schutz, C. Klughammer, C. Griesbeck, A. Quentmeier, C. G. Friedrich and G. Hauska, *Arch. Microbiol.*, 1998, **170**, 353-360.
31. I. T. Cunha, I. F. Teixeira, J. P. Mesquita, J. D. Ardisson, I. Binatti, F. V. Pereira and R. M. Lago, *J. Braz. Chem. Soc.*, 2016, **27**, 363 – 371.
32. I. T. Cunha, I. F. Teixeira, A. S. Albuquerque, J. D. Ardisson, W. A. A. Macedo, H. S. Oliveira, J. C. Tristao, K. Sapag and R. M. Lago, *Catal. Today*, 2015, **259**, 222-227.
33. B. R. S. Lemos, I. F. Teixeira, J. P. Mesquita, R. R. Ribeiro, C. L. Donnici and R. M. Lago, *Carbon*, 2012, **50**, 1386-1393.
34. B. R. S. Lemos, I. F. Teixeira, B. F. Machado, M. R. A. Alves, J. P. Mesquita, R. R. Ribeiro, R. R. Bacsa, P. Serp and R. M. Lago, *J. Mater. Chem., A*, 2013, **33**, 9491-9497.
35. M. C. M. Castro, I. T. Cunha, F. G. Mendonça, R. Augusti, J. P. Mesquita, M. H. Araujo, M. M. Escandell, M. M. Sabio, R. M. Lago and F. R. Reinoso, *Langmuir*, 2017, **33**, 11857-11861.
36. D. Barrera, M. Dávila, V. Cornette, J.C.A. de Oliveira, R. López, K. Sapag, *Micropor. Mesopor. Mater.*, 2013, **180**, 71-78.
37. F. Rouquerol, J. Rouquerol, K. S. W. Sing, P. Llewellyn and G. Maurin, *Adsorption by powders and porous solids: Principles, methodology and applications*, second ed., Academic Press, San Diego, 2014.
38. M. Thommes, K. Kaneko, A.V. Neimark, J.P. Olivier, F.R. Reinoso, J. Rouquerol, and K.S.W. Sing, *Pure Appl. Chem.*, 2015, **87**, 1051-1069.

View Article Online
DOI: 10.1039/C8NJ00922H

39. A. D. Purceno, A. P. C. Teixeira, A. B. Souza, J. D. Ardisson, J. P. Mesquita and R. M. Lago, *Appl. Clay Sci.*, 2012, **69**, 87-92.
40. L. A. Alves, A. H. Castro, F. G. Mendonça and J. P. Mesquita, *Appl. Surf. Sci.*, 2016, **370**, 486-495.
41. D. M. Keown, X. Li, J. I. Hayashi and C. Z. Li, *Energy Fuels*, 2007, **21**, 1816-1821.
42. J. Ribeiro-Soares, M. E. Oliveros, C. Garin, M. V. David, L. G. P. Martins, C. A. Almeida, E. H. Martins-Ferreira, K. Takai, T. Enoki, R. Magalhães-Paniago, A. Malachias, A. Jorio, B. S. Archanjo, C. A. Achete and L. G. Cançado, *Carbon*, 2015, **95**, 646-652.
43. Y. Gokce and Z. Aktas, *Appl. Surf. Sci.*, 2014, **313**, 352-359.
44. H. F. Gorgulho, J. P. Mesquita, F. Gonçalves, M. F. R. Pereira, and J. L. Figueiredo, *Carbon*, 2008, **46**, 1544-1555.
45. D. Lozano-Castello, D. Cazorla-Amoros, A. Linares-Solano, S. Shiraishi, H. Kurihara and A. Oya, *Carbon*, 2003, **41**, 1765-1775.
46. K. Kinoshita, *Electrochemical and Physicochemical Properties*, first ed., John Wiley & Sons, New York, 1987.
47. S. Biniak, A. Swiatkowski and M. Pakula, in: L.R. Radovic (Ed.), *Chemistry and physics of carbon*, Dekker, New York, 2001, vol. 27, pp.125 – 225.
48. S. Xin, L. Gu, N. H. Zhao, Y. X. Yin, L. J. Zhou, Y. G. Guo and L. J. Wan, *J. Am. Chem. Soc.*, 2012, **134**, 18510-18513.

View Article Online
DOI: 10.1039/C8NJ00922H

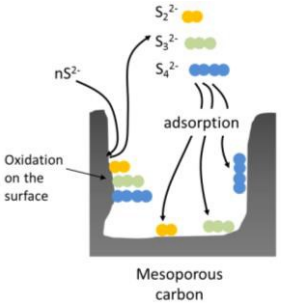

Surface modified mesoporous nanocasting carbon can promote aqueous sulfide oxidation adsorbing produced polysulfides.